IEEE Access
Multidisciplinary | Rapid Review | Open Access Journal

Received April 19, 2021, accepted May 12, 2021, date of publication May 17, 2021, date of current version May 25, 2021.

Digital Object Identifier 10.1109/ACCESS.2021.3081104

Lock-In Based Phase Fluorometric Dissolved Oxygen Sensor Interface With 4 kHz – 150 kHz Tunable Excitation Frequency and Frequency Error Calibration

XUANKAI ZHI[1], YATING ZOU[1], YIZHOU JIANG[1], (Student Member, IEEE), AND YAJIE QIN[1,2], (Member, IEEE)

[1]School of Information Science and Technology, Fudan University, Shanghai 200433, China
[2]State Key Laboratory of ASIC and System, Fudan University, Shanghai 200433, China

Corresponding author: Yajie Qin (yajieqin@fudan.edu.cn)

ABSTRACT Optical dissolved oxygen (DO) concentration measurement based on phase fluorometric theory is one of the most promising DO concentration measurement methods with advantages of insensitivity to the solution, short response time, and satisfying maintainability. However, most phase fluorometric DO concentration measurement systems have limitations such as strong dependence with the chemiluminescent films, low level integration and large noise interference. In this paper, a fully integrated lock-in based phase fluorometric DO sensor interface is proposed with a wide range tunable excitation frequency to be compatible with various chemiluminescent films. The lock-in technique is adopted to improve the sensitivity with large background noise. The proposed interface chip consists of driver for excitation light, transimpedance amplifier (TIA) to read out the weak current of the optical detector, and lock-in amplifier (LIA) for phase-shift detection. A tunable sinusoidal current generator (SCG) based on digital recursive oscillator (RDO) is adopted to generate excitation signal, meeting the requirements of different chemiluminescent films, while a counter-based orthogonal signals generator (OSG) is applied to generate orthogonal demodulating signals. The frequency error between the demodulating signals and excitation signal, which would cause phase-shift detection error, is cancelled by digital calibration method, which relaxes the challenge to match the demodulation signals with the tunable excitation signal. The TIA with DC cancellation is utilized to suppress the DC current of the photodiode (PD) and thus to improve the accuracy of phase-shift detection. The customized interface chip is implemented using a 0.18 μm CMOS process with a core area of 660 μm*464 μm. The test results show that the developed system has an accuracy of 0.06 degrees and a precision of 0.2 degrees in terms of the excitation frequency range from 4 kHz to 150 kHz.

INDEX TERMS Dissolved oxygen, phase fluorometric, tunable excitation frequency, frequency error calibration, lock-in amplifier, digital recursive oscillator, DC cancellation.

I. INTRODUCTION

Dissolved oxygen (DO) concentration is a crucial indicator for water quality and blood health. Measurement systems for DO concentration are widely used in many fields such as aquaculture and biomedical applications. There are three main methods for DO concentration measurement: the iodine titration method (ITM), the Clark oxygen electrode method, and the optical fluorescence quenching method [1]. ITM is commonly adopted in industrial fields since it shows the highest measurement accuracy against others. However, the sensing system and the manual operation for ITM are very complicated, and the response time is particularly long. Besides, the ITM process consumes oxygen in the analyte, and the measurement result is highly affected by other compositions of the solution. Hence the applications of ITM are limited [2], [3]. The Clark electrode method has wider applications and has relatively high measurement accuracy.

The associate editor coordinating the review of this manuscript and approving it for publication was Chao Zuo.

However, the measurement accuracy is also affected by other compositions in solution and the characteristic of electrodes, so it requires frequent manual calibration and maintenance [4], [5]. The optical fluorescence quenching method has high precision and short response time thus can realize real-time measurement. Moreover, its measurement accuracy is almost not affected by other compositions of the solution. The system can be automatically calibrated and does not require frequent maintenance, so it has promising market application prospects [6], [7].

Luminophore quenching can be described by the Stern-Volmer equation [8]:

$$\frac{I_0}{I} = \frac{\tau_0}{\tau} = 1 + K_{SV}[O_2] = 1 + K_Q\tau_0[O_2] \tag{1}$$

where I_0 and τ_0 are the luminescence intensity and lifetime in the absence of O_2, and I and τ are the luminescence intensity and lifetime in the presence of O_2, respectively, K_{SV} is the Stern-Volmer constant, K_Q is the bimolecular quenching constant and $[O_2]$ is the fractional gaseous O_2 concentration. The O_2 concentration influences the luminescence intensity and lifetime of the active agents. The active agents are entrapped in a porous and hydrophobic sol gel film which can convert DO concentration into optical information [9]. In consequence, there are two methods to detect the DO concentration according to Eq. (1): the measurement of luminescence intensity (intensity fluorometry) and the measurement of luminescence lifetime (lifetime fluorometry). [10] and [11] published DO sensors based on intensity fluorometry. It has been proved that these sensors have many drawbacks, including susceptibility to light sources and detector drift, sensitivity to light path fluctuations, and drift resulting from degradation or leaching of fluorescein dyes. These challenges can be minimized by utilizing lifetime fluorometry [12]–[15]. The lifetime is an intrinsic property of luminophores, which is less sensitive to optical devices drifts and light path fluctuations. Therefore, lifetime fluorometry is often preferred for the design of reliable luminescence-based DO sensors. However, the direct measurement of luminescence lifetime needs high speed signal detection and processing circuits because the lifetime is relatively short.

To simplify the lifetime measurement, the phase fluorometry technique is introduced to monitor DO concentration [16]. Phase fluorometry can convert luminescence lifetime to the phase shift between the luminescence signal and the excitation signal, which only requires signal detection and processing instruments with lower bandwidth and sampling rate. Thus, it has become a promising method to replace direct lifetime measurements. The lifetime τ and the corresponding phase shift φ [17] follows

$$\tan\varphi = 2\pi f\tau \tag{2}$$

where f is the frequency of excitation signal. The phase shift between the luminescence signal and excitation signal is illustrated in Fig. 1. Many DO sensors based on phase fluorometry with various means of phase detection have been

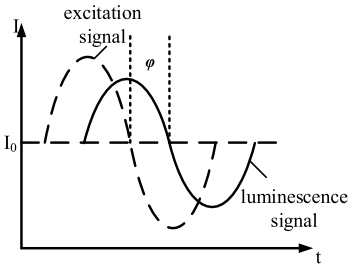

FIGURE 1. Principle of phase fluorometric method.

reported [18]–[21]. In [16] and [18], frequency-domain fluorescence lifetime DO sensors with XOR-gate and low-pass filter (LPF) based phase detector were introduced. Despite the cost-effectiveness and power-efficiency, the XOR-gate and LPF based phase-to-voltage conversion topology suffers from poor resolution and small dynamic range, which is inherently due to poor swings under low power supply voltages. To collect weak optical signals which often suffers severe noise interference, the lock-in technique is raised, that can realize high precision for optical interface compared to XOR-gate based ones. A portable analog lock-in amplifier (LIA) for accurate phase detection was proposed to realize good noise performance in [22], yielding 0.1 degrees precision. [23] presented an optical DO measurement method based on a fast digital lock-in algorithm that realizes a precision of 0.01 degrees. LIAs based on discrete commercial electronic components have shown encouraging results and are suggested suitable for use in many sensing devices. Unfortunately, LIAs based on discrete components often have high costs, large sizes and weights, so they are not suitable for portable sensor systems. A fully integrated analog LIA for the accurate detection and measurement of small, slow, and noisy signals was presented in [24]. In conclusion, many efforts have been made on the optimization of the receiver part in lock-in systems.

Besides the receiver, the transmitter is also an essential part of the system. However, few works have been reported to optimize the transmitter part, and the existing transmitters are generally not integrated inside the optical DO sensor interface chip. A typical transmitter mainly consists of a sinusoidal current generator (SCG) and an orthogonal signals generator (OSG). In phase fluorometry systems, with increasing modulation frequency, signal-to-noise ratio (SNR) of modulated signal decreases, but the phase sensitivity improves [8]. Therefore, it is necessary to select an optimized excitation frequency according to the fluorescence lifetime of particular chemiluminescent films [19]. Thus, a current excitation signal with tunable frequency is required in DO sensing systems. The SCGs based RC oscillator [25], [26] can achieve superior total harmonic distortion (THD) performance but consume huge power, occupy large area, and have poor frequency accuracy. Variable-frequency lock-in detection using direct digital synthesizer (DDS) [27] was proposed for higher frequency accuracy, but it requires a large memory area. The OSG is adopted to generate the demodulating signals,

which should be synchronized with the excitation signal. The frequency error between excitation signal and demodulating signals leads to phase-shift detection error. [28] presented an effective but complex circuit, i.e., a digital LIA with accurate frequency automatic tracking to avoid the frequency error. In DDS based transmitters, the demodulating signals can be achieved by simple counters.

To overcome the limitations mentioned above, this paper presents a fully integrated lock-in based phase fluorometric DO sensor interface system with wide range tunable excitation frequency. A variable-frequency SCG based on the digital recursive oscillator (RDO) [29] is used to drive the LED, making the system adapt to various chemiluminescent films. The lock-in technique is adopted to suppress noise and eliminate the influence of dark current. A digital counter-based OSG is used to generate the orthogonal demodulating signal. Although it has frequency error with the excitation signal, a foreground calibration is proposed in this paper to cancel the phase-shift detection errors caused by it, which guarantees a relatively high accuracy while consuming less power and area.

The remainder of this paper is organized as follows. Section II introduces detection principle and architecture of the proposed phase fluorometric DO sensor interface system. Section III gives the detailed circuits design. Section IV shows the experiment results, and Section V draws a conclusion.

II. DETECTION PRINCIPLE AND SYSTEM ARCHITECTURE

A. The PRINCIPLE OF LIA

Fig. 2 shows the block diagram of the lock-in technique. The input signal can be expressed as

$$V_{in} = A\cos(\omega_1 t + \varphi) + n(t) \quad \omega_1 = 2\pi f_{osc} \tag{3}$$

where f_{osc} is the frequency of input signal, A is the amplitude of input signal, $n(t)$ is the input noise, and φ is the phase shift. The demodulating signal, *vclki*, is expressed as

$$vclki = B\{\frac{1}{2} + \frac{2}{\pi}\sum_{n=1}^{\infty}\frac{(-1)^{n+1}}{2n-1}\cos[(2n-1)\omega_2 t]\}\omega_2 = 2\pi f_c \tag{4}$$

where B is the amplitude of *vclki*, f_c is the frequency of *vclki*. The output of mixer can be expressed as

$$\begin{aligned} V_I &= [A\cos(\omega_1 t + \varphi) + n(t)] \\ &\quad * B\{\frac{1}{2} + \frac{2}{\pi}\sum_{n=1}^{\infty}\frac{(-1)^{n+1}}{2n-1}\cos[(2n-1)\omega_2 t]\} \\ &= n(t) * B\{\frac{1}{2} + \frac{2}{\pi}\sum_{n=1}^{\infty}\frac{(-1)^{n+1}}{2n-1}\cos[(2n-1)\omega_2 t]\} \\ &\quad + \frac{AB}{2}\cos(\omega_1 t + \varphi) \\ &\quad + \frac{AB}{\pi}\sum_{n=1}^{\infty}\frac{(-1)^{n+1}}{2n-1}\cos[(2n-1)\omega_2 t - \omega_1 t - \varphi] \end{aligned}$$

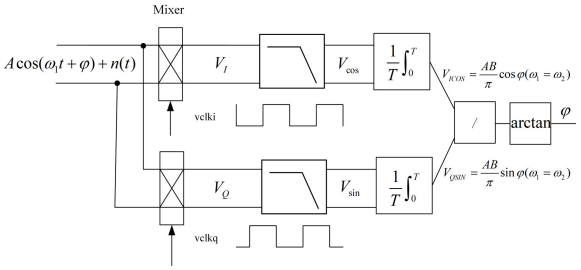

FIGURE 2. The block scheme of the lock-in technique.

$$+\frac{AB}{\pi}\sum_{n=1}^{\infty}\frac{(-1)^{n+1}}{2n-1}\cos[(2n-1)\omega_2 t + \omega_1 t + \varphi] \tag{5}$$

Then, since cutoff frequency of LPF is much lower than ω_1 and ω_2, the high-frequency components will be removed. When $\omega_1 = \omega_2$, the output of LPF can be expressed as

$$V_{\cos} = \frac{AB}{\pi}\cos\varphi + B\{\frac{1}{2} + \frac{2}{\pi}\sum_{n=1}^{\infty}\frac{(-1)^{n+1}}{2n-1} \times \cos[(2n-1)\omega_2 t]\}n(t) \tag{6}$$

According to the principle of correlation, the influence of noise can be eliminated by averaging the above signals over a certain period of time.

$$\frac{1}{T}\int_0^T B\{\frac{1}{2} + \frac{2}{\pi}\sum_{n=1}^{\infty}\frac{(-1)^{n+1}}{2n-1}\cos[(2n-1)\omega_2 t]\}n(t)dt = 0 \tag{7}$$

So, the final output of the I/Q channel is

$$V_{ICOS} = \frac{AB}{\pi}\cos\varphi \quad V_{QSIN} = \frac{AB}{\pi}\sin\varphi \tag{8}$$

Then φ can be calculated through

$$\varphi = \arctan\frac{V_{QSIN}}{V_{ICOS}} \tag{9}$$

B. SYSTEM ARCHITECTURE

The block diagram of lock-in based DO sensor system is depicted in Fig. 3. The whole system is mainly composed of transmitter, sensor part, receiver, and digital processing and control unit.

The sensor part is composed of two LEDs, the DO solution, fluorescent film, an optical filter (OF), and a photodiode (PD). Excitation signal generated by SCG drives blue LED (BLED) to emit the blue light which excites the chemiluminescent films to emit the red luminescence. The light signal filtered by the OF is detected and transformed into current signal referred as modulated fluorescence signal by PD. If the excitation signal is a sinusoidal signal, the modulated fluorescence signal will have a phase shift with the excitation signal. The phase shift is linear with DO concentration of the solution when the BLED is driven by a 0 – 20 mA – current [30], but the phase shift will be constant when RLED is the excitation one. The function of sensor part is converting DO concentration to phase shift.

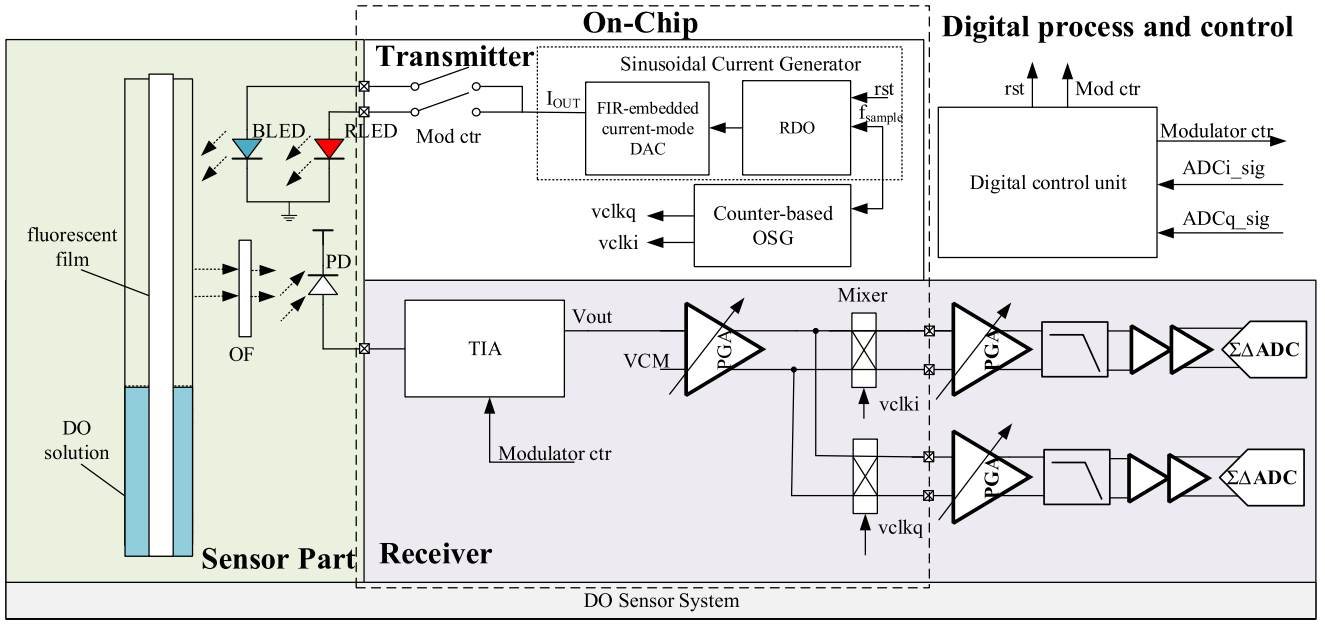

FIGURE 3. The block diagram of DO sensor system.

As for the transmitter, it consists of SCG, OSG and switches. The excitation current signal is generated by SCG, whose frequency range is designed to be 4 kHz – 150 kHz, covering most commonly used chemiluminescent films. The amplitude of the excitation current should be 0 – 20 mA to drive the LEDs. The lock-in principle can relax the linearity requirement of SCG. The RDO-based SCG is used in this paper for its small power consumptions and area. Meanwhile, the counter-based OSG is proposed to generate demodulating signal for the mixer. Although, the frequency error between excitation signal and demodulating signal is caused by this way, phase-shift detection errors caused by frequency error can be calibration.

Assuming the excitation frequency is not equal to the demodulating frequency ($\omega_1 \neq \omega_2$), the output of I channel is

$$V'_{ICOS} = \frac{AB}{\pi} \cos\left[(\omega_1 - \omega_2)\, t + \varphi\right] \tag{10}$$

As shown, the output of I channel is not a DC value. To determine the phase difference and eliminate phase error of the circuit and optical path the excitation BLED and reference RLED are alternately switched. The phase error coming from frequency error can also be eliminated when the reset signal (*rst*) of RDO is synchronized with the switch control signal (*Mod ctr*). The principle is illustrated in Fig. 4. When the BLED is the excitation source, the modulated fluorescence signal is the sensing signal, V_{sig}. The modulated fluorescence signal is the reference signal, V_{ref}, when RLED is the excitation one. Those signals can be expressed as

$$\begin{aligned} V_{sig} &= A\cos(\omega_1 t + \omega_1 T_1 + \varphi_{DO} + \varphi_0) \\ V_{ref} &= A\cos(\omega_1 t + \omega_1 T_2 + \varphi_0) \end{aligned} \tag{11}$$

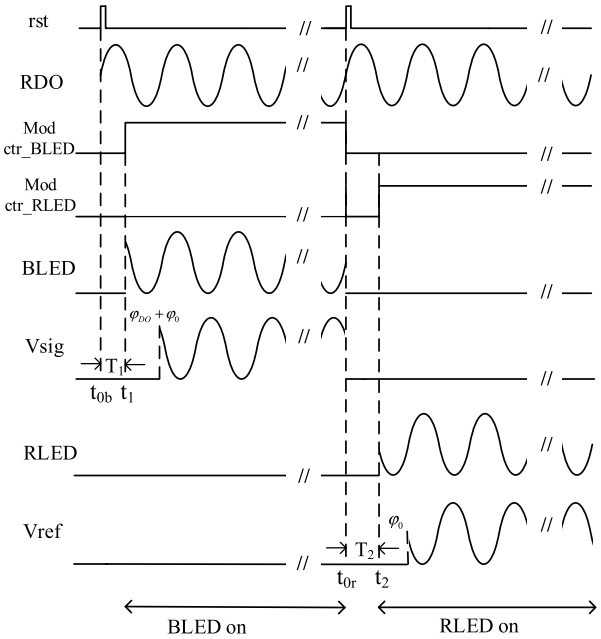

FIGURE 4. The time diagram of frequency error calibration.

where φ_0 is the phase shift of the circuit and optical path, φ_{DO} is the phase shift caused by the chemiluminescent film. The phase shift detection output of sensing signal, φ_b, and reference signal, φ_r, can be expressed as

$$\begin{aligned} \varphi_b &= (\omega_1 - \omega_2)t + \omega_1 T_1 + \varphi_{DO} + \varphi_0 \\ \varphi_r &= (\omega_1 - \omega_2)t + \omega_1 T_2 + \varphi_0 \end{aligned} \tag{12}$$

where t_{0b}, t_{0r} are the reset time of RDO. The initial phase of RDO at reset time is constant. t_1 is the turn on time of BLED, t_2 is turn on time of RLED. The measured phase shift φ_{DO} can be extracted through $\varphi_b - \varphi_r$. When rst is synchronized with

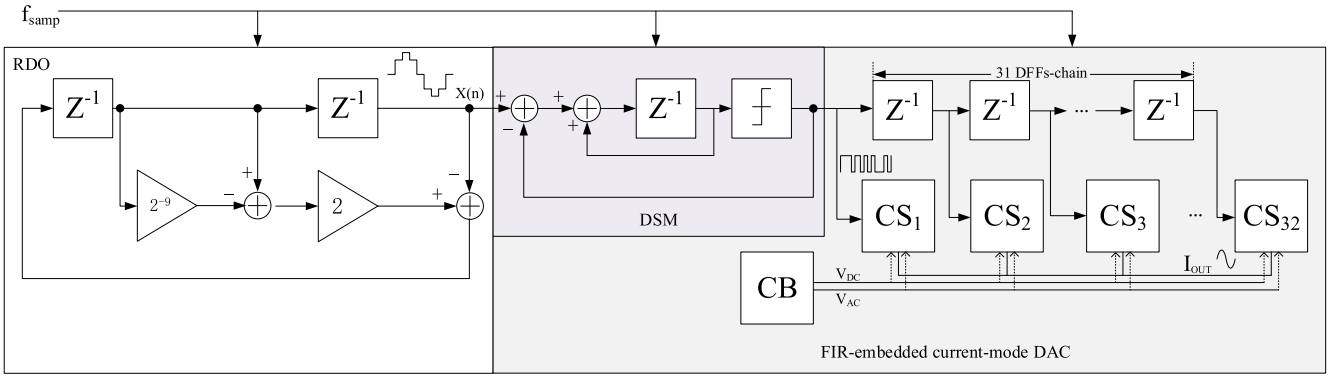

FIGURE 5. The circuit diagram of the sinusoidal current generator.

the Mod ctr, $T_1 = T_2$, the frequency error can be eliminated. To guarantee the effectiveness of frequency error elimination the frequency error $(\omega_1 - \omega_2)$ should not be higher than the cutoff frequency of LPF. Therefore, the frequency error between excitation and demodulating signals should be lower than 1%, considering the trade-off with LPF design.

For the receiver, the modulated fluorescence signal is converted into voltage signal by a transimpedance amplifier (TIA). The modulated fluorescence signal is a sinusoidal current signal with DC current. The value of DC current is 0 – 7.5 μA when LED is driven by 0 – 20 mA current. The DC current is irrelevant to the phase signal. To improve the gain and linearity of the TIA, a DC cancellation TIA scheme is adopted. A fully differential programmable gain amplifier (PGA) is adopted to reduce the load capacity requirement of TIA and improve the linearity of TIA. The lock-in amplifier is used to reduce the influence of dark current of PD. The gain of TIA and PGA can be configured by the digital control unit.

Finally, the digital process and control unit receives the analog-to-digital converter (ADC) output. And the phase shift is calculated with the coordinate rotation digital computer (CORDIC) algorithm. The switch-control signal and reset signal are also generated by this unit.

III. CIRCUITS DESIGN

A. TRANSMITTER

Fig. 5 shows the circuit diagram of a sinusoidal current generator which consists of an RDO, FIR-embedded current-mode DAC [26]. To realize wide range tunable excitation frequency and reduce power consumption and area, the RDO is adopted in place of DDS. The RDO uses the second-order digital filter structure that generates successive samples of a single sinusoidal waveform. The circuit diagram is shown in Fig. 5. Its difference equation form is expressed as

$$x(n+2) = \lambda \cdot x(n+1) - x(n), \quad n \geq 0 \tag{13}$$

The unit sample response of Eq. (13) is expressed as

$$x(n) = \cos\left(n\phi_{osc} + \varphi\right), \quad \phi_{osc} = 2\pi \cdot f_{osc}/f_{samp} \tag{14}$$

where φ is the initial phase, which is decided by the initial value of *x(0)*, *x(1)* and the coefficient λ. f_{osc} and f_{samp} are sinusoidal output frequency and sampling clock frequency. In this design, the initial values of *x(1)* and *x(0)* are selected as $\cos\phi_{osc}$ and 1, and the coefficient λ is selected as $2\cdot\cos\phi_{osc}$ to ensure the initial phase is zero, the f_{osc} is initially set to 1/100 of the f_{samp}, the initial value of *x(1)* and λ can be calculated as approximately 0.9980265 and 1.996053. To simplify the digital circuit implementation, *x(1)* and λ are set to $1\text{-}2^{-9}$ and $2 \cdot (1 - 2^{-9})$ which cause a 0.5% frequency error.

The 1st order DSM provides 1-bit output of the RDO, modulate the noise to high frequency. The DSM output is then shifted to the next D-flip flop (DFF) at every f_{samp} cycle along the 31-DFFs chain, and each DFF output controls the output polarity of each differential current source (CS_{1-32}). Each output act as each tap of FIR filter. The structure of CS and current bias (CB) is shown in Fig. 5. The output current can be adjusted by changing the value of V_{AC} and V_{DC}. In the attempt to drive the LEDs, the equivalent impedance of switch R_{sw} should be designed as low as possible. Here R_{sw} presents $<100\Omega$ resistance to achieve better trade-off.

In order to demodulate the phase signal, this paper uses a counter-based OSG to generate the orthogonal demodulating signal. The counter uses the same sampling clock with the SCG. Frequency division is used by counter to generate orthogonal signals. It is very easy to generate a pair of orthogonal demodulating signals with good orthogonality in this way. However, the frequency of I_{OUT} has 0.5% frequency error with the demodulating signal. The effect of frequency errors on phase measurements can be eliminated by frequency error calibration.

B. RECEIVER

The PD output is a sinusoidal signal with DC current $(i_{AC} + I_{DC})$. The DC current is irrelated to the measurement signal. To improve the gain and linearity of the TIA, a DC cancellation TIA is adopted. The circuit diagram of the TIA is shown in Fig. 6. The range of the PD DC current (I_{DC}) is 0 – 7.5 μA. To eliminate DC current among such a wide current range, a 4-bit DAC is used. The maximum range of DC elimination is 12 μA and the precision of 0.8 μA is achieved. To realize automatic cancellation, two comparators are used for amplitude monitoring. The comparator detects the output

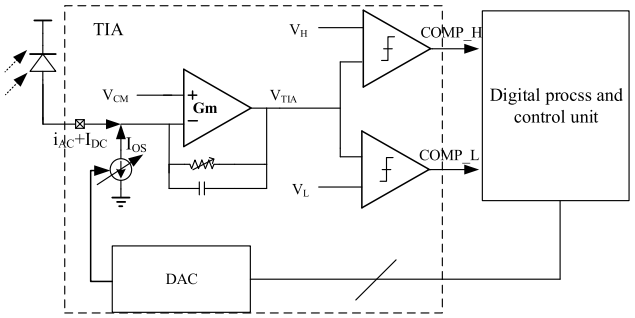

FIGURE 6. The circuit diagram of the TIA.

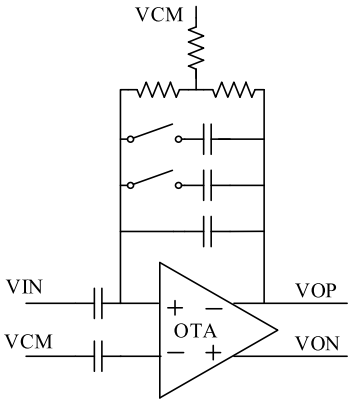

FIGURE 7. The half circuit structure of PGA.

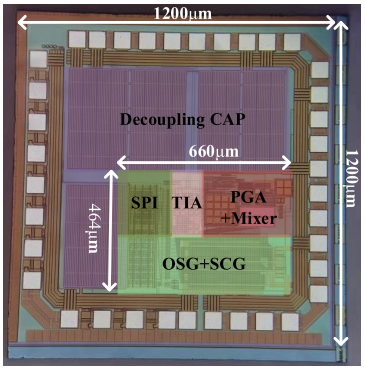

FIGURE 8. Chip microphotograph of the proposed DO sensor interface.

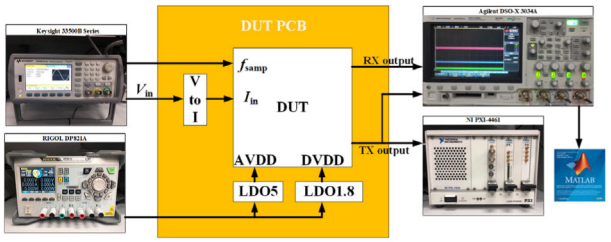

FIGURE 9. Platform of the proposed DO sensor interface system.

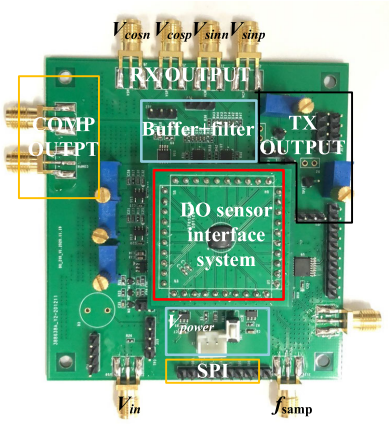

FIGURE 10. Photo of the PCB for measurement.

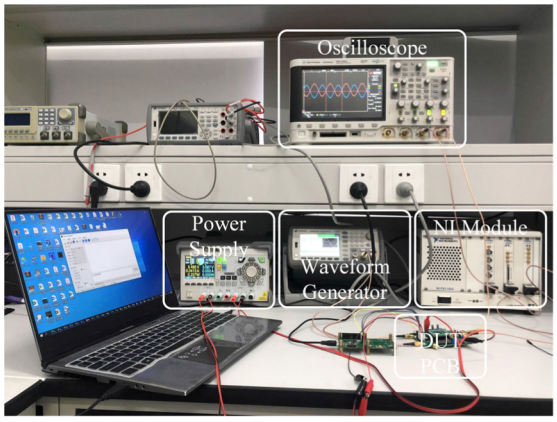

FIGURE 11. Experimental setup.

voltage of the TIA (V_{TIA}) and then compares it with the threshold voltages V_H and V_L. If $V_{TIA} > V_H$ or $V_{TIA} < V_L$, flag signals (*COMP_H*, *COMP_L*) will be generated, which indicates that the input residual DC is not small enough. Thus, the digital process and control unit detects the flag and changes the configurable work to increase I_{OS}. This negative feedback loop guarantees $V_L < V_{TIA} < V_H$. Considering the precision of comparator, the reference voltages of the two comparators were set at 0.7 V and 4.3 V respectively to achieve a TIA output range of 0.5 V – 4.5 V.

The PGA works as a bandpass filter and drives the mixer. The PGA circuit architecture is shown in Fig. 7. The proposed full differential PGA uses a capacitive-feedback topology which utilizes a capacitor to set the passband gain and to reject the DC offset from the TIA. The core amplifier of the PGA adopts a two-stage fully differential folded-cascode architecture to achieve high common mode rejection ratio (CMRR) and power supply rejection ratio (PSRR) [31]. The passband gain of the amplifier is set by the ratio between the input capacitor, C_{in}, and the feedback capacitor, C_f, which can be digitally controlled by adjusting the feedback capacitor. The gain increases linearly in a dB-scale from 0 to 12 dB in 6 dB steps. A DC feedback path is provided by the feedback resistor R_f. R_f is achieved by the t-resistance network rather than the MOS-BJT pseudo-resistor, since t-resistance is more stable and has a larger dynamic range. Such structure can realize resistance larger than $10^7\Omega$ while occupying small area. The low cutoff frequency, f_L, is set by $1/(2\pi R_f C_f)$. The frequency range of signal is 4 kHz – 150 kHz, so the low cutoff frequency should be lower than 4kHz.

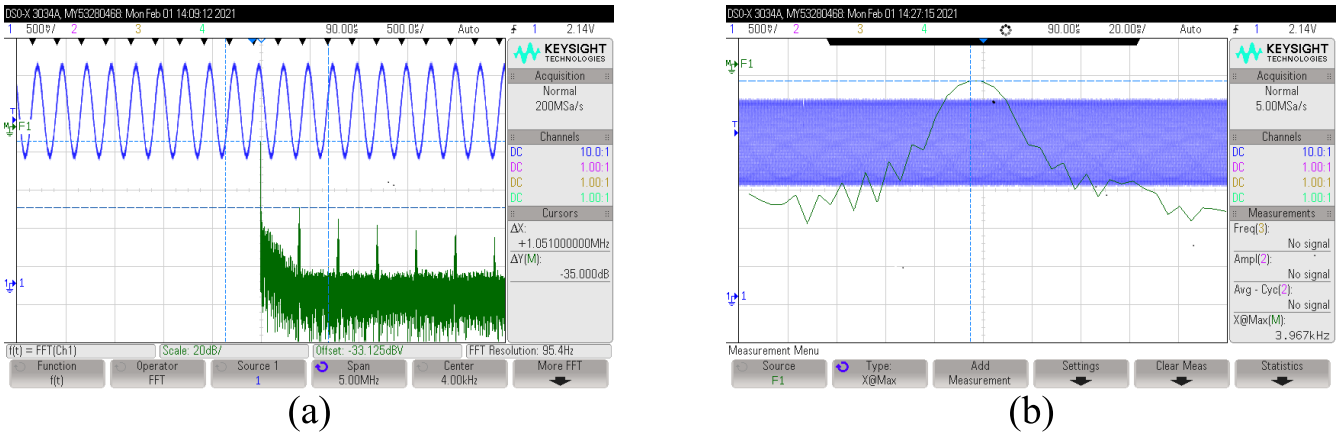

FIGURE 12. Output of SCG. (a) Output waveforms in time domain and frequency-domain. (b) Frequency of output.

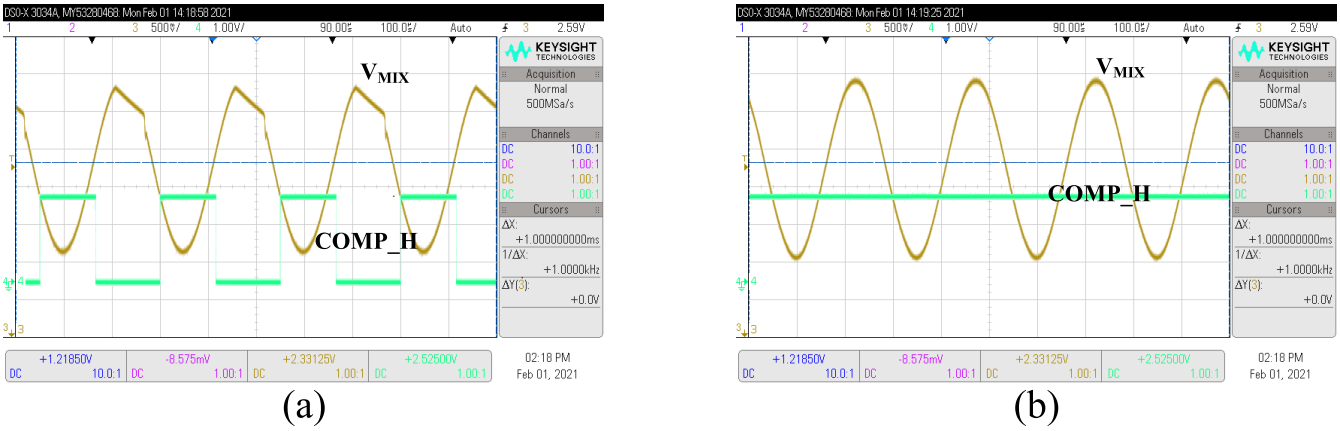

FIGURE 13. Output of TIA (a) Without DC cancellation. (b) With DC cancellation.

IV. EXPERIMENTS AND RESULTS

A. TEST ENVIRONMENT

The chip was implemented with the 0.18 μm CMOS technology. Fig. 8 depicts the microphotograph of the proposed DO sensor interface chip. The area of whole chip is 1200 μm $*$ 1200 μm. The core area is approximately 660 μm $*$ 464 μm. The current source in the FIR-embedded current-mode DAC occupies most of the chip area. The performances of the DO system were measured under a 5 V analog supply voltage.

Fig. 9 presents the measurement platform, including printed circuit board (PCB) (see Fig. 10) with device under test (DUT). A sampling signal f_{samp} (400 kHz – 15 MHz), and a sinusoidal voltage signal V_{in} (4 kHz – 150 kHz) are set using a waveform generator (Keysight 33520B). The sinusoidal voltage signal is converted via a V-to-I module to the current signal I_{in}.

The outputs of the receiver (V_{cosn}, V_{cosp}, V_{sinn}, V_{sinp}) and the output of transmitter (TX output) are acquired and collected by digital storage oscilloscope (Agilent DSO-X 3034A) and processed in MATLAB. The output signals of receiver are also captured with a high resolution dynamic signal acquisition module (NI PXI-4461) and imported into the MATLAB environment for calculation of the angle. The experimental setup is shown in Fig. 11.

B. TESTS AND RESULTS OF SCG AND TIA WITH DC CACELLATION

A 150 Ω resistor and a 1 nF capacitor in parallel, were used to model the LED according to the datasheet [30] when the output current of the SCG was measured. As illustrated in Fig. 12, the SFDR of the SCG output is 35 dB and it can be further increased with larger capacitor. The output frequency is 3.967 kHz when the f_{samp} is set as 400 kHz. The frequency error is less than 0.8% when the f_{samp} frequency is tuned from 400 to 1500 kHz.

In order to test the DC cancellation function of TIA, the current signal of I_{in} is set to be 5μApp AC with 7.5 μA DC offset. Meanwhile, *vclki* and *vclkq* are set to 5 V to disable the mixer. Fig. 13(a) shows the output of mixer (V_{MIX}) without DC cancellation. When the output of TIA (V_{out}) is higher than V_H, there is an obvious distortion due to large DC current, and the comparator has a periodic digital output (*COMP_H*). When the digital process and control unit detects the rising edge of *COMP_H*, the DC cancellation works. Then, the V_{out}

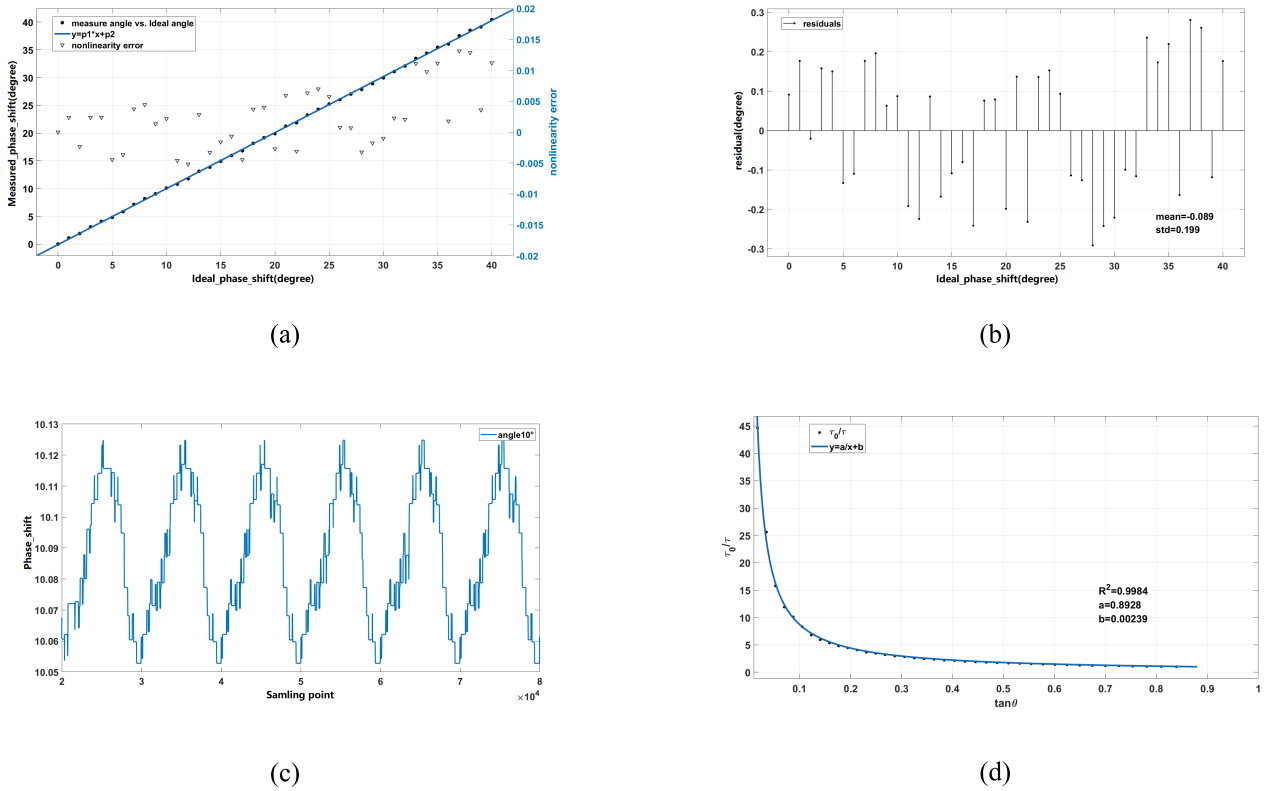

FIGURE 14. (a) Linear output and nonlinearity characteristics of the measured phase. (b) The relationship between the residual and the ideal angle. (c) Measurement results of 10 degrees for a period of time. (d) The relationship between the phase difference and τ_0/τ.

is adjusted to be lower than V_H. And the output signal shows great linearity as can be seen on Fig. 13(b).

C. PHASE SHIFT DETECTION TEST

The current signal without frequency error (I_{in}) is given to the input of receiver as a reference signal to calculate the phase, θ_{ref}. And then, a signal with predefined phase difference is given as a sensing signal to calculate the phase, θ_{se}. The measured phase shift can be expressed as θ_{se}-θ_{ref}.

The test results are shown in Fig. 14. The relationship between the measured phase shift and the ideal phase shift is shown in Fig. 14(a). It is observed from the figure that the worst-case error from the best linear fit is 1.5%, thereby indicating a good degree of linearity. Fig. 14(b) shows the relationship between the residual with the ideal angle. The precision of the DO sensor system is 0.2 degrees. In Fig. 14(c), the measurement of 10 degrees phase shift was tested for a period of time. Because of the noise and harmonic, the phase measurements have a certain extent of drift during the measuring time. The phase ranges from 10.06 degrees to 10.12 degrees, and the accuracy of phase measurement is 0.06 degrees.

The relationship between the phase shift and τ_0/τ is presented in Fig. 14(d). Therefore, as the relationship between the DO concentration with the τ_0/τ is known, the DO concentration could be calculated using the phase shift.

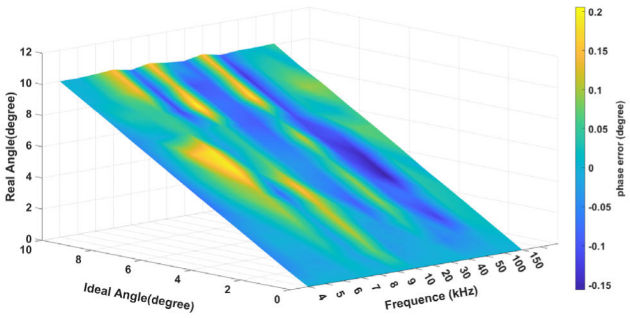

FIGURE 15. The phase error versus different frequency.

Since the frequency of I_{in} is adjusted from 4 kHz to 150 kHz. The phase error is tested over the whole frequency range. The result is shown in Fig. 15. The DO system can realize the precision of 0.2 degrees when the frequency range is 4 kHz – 150 kHz.

D. MEASUREMENT RESULTS OF FREQUENCY ERROR CALIBRATION

The reference and sensing current signal with the same frequency as the TX output is given to the input of receiver. As can be seen in Fig. 16, the output signal of the filter is not a DC value but a sawtooth wave, and the frequency of the sawtooth wave is the same as the frequency error between the excitation signal and demodulating signal.

TABLE 1. Performance summary and comparison with other DO sensors interfaces.

Ref (year)	[16] (2001)	[21] (2017)	[22] (2020)	[18] (2007)	[14] (2018)	[32] (2014)	This work
Technology	N/A	N/A	N/A	1.5μm CMOS	0.18μm CMOS	N/A	0.18μm CMOS
Implementation	Discrete components	Discrete components	Discrete components	IC	IC	N/A	IC
Supply voltage(V)	N/A	N/A	12	5	1.8	N/A	5
Technique	frequency	frequency	frequency	frequency	charge modulation	frequency	frequency
Modulation Frequency (kHz)	20	16	5	5-1000	5	N/A	4-150
Phase detection	XOR-gate based	Analog lock-in	Digital lock-in	XOR-gate based	N/A	Lock-in	Analog lock-in with frequency error calibration
Accuracy(degree)	N/A	N/A	0.01	N/A	N/A	N/A	0.06
Precision(degree)	<2	0.1	N/A	<5	0.081	N/A	0.2
Oxygen resolution (mg/L)	0.01	N/A	N/A	N/A	0.06	0.01	N/A
Area(mm^2)	N/A	N/A	N/A	4.84	2.25	N/A	1.44
Power(mW)	N/A	N/A	N/A	80	1.44	N/A	75*

*LED driver is integrated in the chip

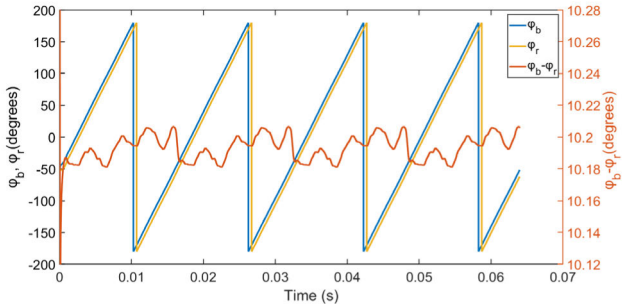

FIGURE 16. The phase shift with frequency error.

So, the phase obtained from the CORDIC algorithm changes periodically over time, as shown in Fig. 16. When the reset signal of RDO is used as two alternating conduction control signals for LEDs, the output phase is subtracted from the reference phase to obtain the measured phase. As seen in the Fig. 16, the precision of the phase measurement is 0.2 degrees and the accuracy is 0.04 degrees when the test phase shift is 10 degrees. This result proves that the influence of frequency error can be calibrated.

V. CONCLUSION

This paper has presented a fully integrated lock-in based phase fluorometric DO sensor interface system with wide range tunable excitation frequency and frequency error calibration. The system is integrated with the SCG for LED driving and a detecting and processing integrated circuit. The system uses the lock-in principle to eliminate the influence of noise, frequency error calibration to eliminate the effect of frequency error on phase precision. This system can be applied to measure DO concentration and have many advantages compared with the existing sensors. A comparison study of the proposed sensor interface with the existing DO sensors interfaces is given in Table 1. The LED driver is integrated in the proposed chip and makes the system smaller than other systems. The system can calibrate frequency error, so it does not need the high precision oscillator (e.g., DDS) and high precision OSG to generate the excitation signal and demodulating signal. Instead, only the simple RDO circuit and counter are needed. The proposed system has an accuracy of 0.06 degrees and a precision of 0.2 degrees at the frequency range of 4 kHz – 150 kHz, enabling it to be a promising sensor for phase detection applications.

REFERENCES

[1] Y. Wei, Y. Jiao, D. An, D. Li, W. Li, and Q. Wei, "Review of dissolved oxygen detection technology: From laboratory analysis to online intelligent detection," *Sensors*, vol. 19, no. 18, p. 3995, Sep. 2019.
[2] I. Helm, L. Jalukse, and I. Leito, "A highly accurate method for determination of dissolved oxygen: Gravimetric winkler method," *Anal. Chim. Acta*, vol. 741, pp. 21–31, Sep. 2012.
[3] A. Shriwastav, G. Sudarsan, P. Bose, and V. Tare, "A modified winkler's method for determination of dissolved oxygen concentration in water: Dependence of method accuracy on sample volume," *Measurement*, vol. 106, pp. 190–195, Aug. 2017.
[4] H. Suzuki, A. Sugama, and N. Kojima, "Micromachined Clark oxygen electrode," *Sens. Actuators B, Chem.*, vol. 10, no. 2, pp. 91–98, Jan. 1993.
[5] J. Luo, T. Dziubla, and R. Eitel, "A low temperature co-fired ceramic based microfluidic Clark-type oxygen sensor for real-time oxygen sensing," *Sens. Actuators B, Chem.*, vol. 240, pp. 392–397, Mar. 2017.
[6] F. Li, Y. Wei, Y. Chen, D. Li, and X. Zhang, "An intelligent optical dissolved oxygen measurement method based on a fluorescent quenching mechanism," *Sensors*, vol. 15, no. 12, pp. 30913–30926, Dec. 2015.
[7] H. Välimäki, J. Verho, J. Kreutzer, D. K. Rajan, T. Ryynänen, M. Pekkanen-Mattila, A. Ahola, K. Tappura, P. Kallio, and J. Lekkala, "Fluorimetric oxygen sensor with an efficient optical read-out for *in vitro* cell models," *Sens. Actuators B, Chem.*, vol. 249, pp. 738–746, Oct. 2017.
[8] J. R. Lakowicz, *Principles of Fluorescence Spectriscopy*, 3rd ed. New York, NY, USA: Springer, 2006.
[9] N. Shehata, K. Meehan, I. Ashry, I. Kandas, and Y. Xu, "Lanthanide-doped ceria nanoparticles as fluorescence-quenching probes for dissolved oxygen," *Sens. Actuators B, Chem.*, vol. 183, pp. 179–186, Jul. 2013.
[10] C.-S. Chu and Y.-L. Lo, "A plastic optical fiber sensor for the dual sensing of temperature and oxygen," *IEEE Photon. Technol. Lett.*, vol. 20, no. 1, pp. 63–65, Jan. 1, 2008.

[11] C.-S. Chu, T.-W. Sung, and Y.-L. Lo, "Enhanced optical oxygen sensing property based on Pt(II) complex and metal-coated silica nanoparticles embedded in sol–gel matrix," *Sens. Actuators B, Chem.*, vol. 185, pp. 287–292, Aug. 2013.
[12] J. Guo and S. Sonkusale, "A 65 nm CMOS digital phase imager for time-resolved fluorescence imaging," *IEEE J. Solid-State Circuits*, vol. 47, no. 7, pp. 1731–1742, Jul. 2012.
[13] P. Chen, Z. Zhao, D.-D. Zhao, Y.-Y. Han, and R.-H. Liang, "Detection method of dissolved oxygen concentration in water based on single source frequency domain fluorescence lifetime," *Acta Photonica Sinica*, vol. 49, no. 3, 2020, Art. no. 330002.
[14] G. Fu and S. R. Sonkusale, "A CMOS luminescence intensity and lifetime dual sensor based on multicycle charge modulation," *IEEE Trans. Biomed. Circuits Syst.*, vol. 12, no. 3, pp. 677–688, Jun. 2018.
[15] S. Sonmezoglu and M. M. Maharbiz, "A 4.5 mm^3 deep-tissue ultrasonic implantable luminescence oxygen sensor," in *IEEE Int. Solid-State Circuits Conf. (ISSCC) Dig. Tech. Papers*, San Francisco, CA, USA, Feb. 2020, pp. 454–456.
[16] C. McDonagh, C. Kolle, A. K. McEvoy, D. L. Dowling, A. A. Cafolla, S. J. Cullen, and B. D. MacCraith, "Phase fluorometric dissolved oxygen sensor," *Sens. Actuators B, Chem.*, vol. 74, nos. 1–3, pp. 124–130, Apr. 2001.
[17] M. E. Lippitsch and S. Draxler, "Luminescence decay-time-based optical sensors: Principles and problems," *Sens. Actuators B, Chem.*, vol. 11, nos. 1–3, pp. 97–101, Mar. 1993.
[18] V. P. Chodavarapu, D. O. Shubin, R. M. Bukowski, A. H. Titus, A. N. Cartwright, and F. V. Bright, "CMOS-based phase fluorometric oxygen sensor system," *IEEE Trans. Circuits Syst. I, Reg. Papers*, vol. 54, no. 1, pp. 111–118, Jan. 2007.
[19] C.-S. Chu, K.-Z. Lin, and Y.-H. Tang, "A new optical sensor for sensing oxygen based on phase shift detection," *Sens. Actuators B, Chem.*, vol. 223, pp. 606–612, Feb. 2016.
[20] K. Kishore and S. A. Akbar, "Evolution of lock-in amplifier as portable sensor interface platform: A review," *IEEE Sensors J.*, vol. 20, no. 18, pp. 10345–10354, Sep. 2020.
[21] L. Yao, R. Khan, V. P. Chodavarapu, V. S. Tripathi, and F. V. Bright, "Sensitivity-enhanced CMOS phase luminometry system using xerogel-based sensors," *IEEE Trans. Biomed. Circuits Syst.*, vol. 3, no. 5, pp. 304–311, Oct. 2009.
[22] X. Chen, J. Chang, F. Wang, Z. Wang, W. Wei, Y. Liu, and Z. Qin, "A portable analog lock-in amplifier for accurate phase measurement and application in high-precision optical oxygen concentration detection," *Photonic Sensors*, vol. 7, no. 1, pp. 27–36, Mar. 2017.
[23] B. Xia, G. Li, L. Cui, L. Lin, J. Zhang, H. Liao, and Y. Deng, "Method for online high-precision seawater dissolved oxygen measurement based on fast digital lock-in algorithm," *J. Coastal Res.*, vol. 104, no. 1, pp. 216–222, Oct. 2020.
[24] A. De Marcellis, G. Ferri, and A. D'Amico, "One-decade frequency range, in-phase auto-aligned 1.8 V 2 mW fully analog CMOS integrated lock-in amplifier for small/noisy signal detection," *IEEE Sensors J.*, vol. 16, no. 14, pp. 5690–5701, Jul. 2016.
[25] S. Hong, K. Lee, U. Ha, H. Kim, Y. Lee, Y. Kim, and H.-J. Yoo, "A 4.9 mΩ-sensitivity mobile electrical impedance tomography IC for early breast-cancer detection system," *IEEE J. Solid-State Circuits*, vol. 50, no. 1, pp. 245–257, Jan. 2015.
[26] A. Hedayatipour, S. Aslanzadeh, S. H. Hesari, M. A. Haque, and N. McFarlane, "A wearable CMOS impedance to frequency sensing system for non-invasive impedance measurements," *IEEE Trans. Biomed. Circuits Syst.*, vol. 14, no. 5, pp. 1108–1121, Oct. 2020.
[27] M. Ayat, M. A. Karami, S. Mirzakuchaki, and A. Beheshti-Shirazi, "Design of multiple modulated frequency lock-in amplifier for tapping-mode atomic force microscopy systems," *IEEE Trans. Instrum. Meas.*, vol. 65, no. 10, pp. 2284–2292, Oct. 2016.
[28] C. Zhang, H. Liu, J. Ge, and H. Dong, "FPGA-based digital lock-in amplifier with high-precision automatic frequency tracking," *IEEE Access*, vol. 8, pp. 123114–123122, 2020.
[29] S.-K. Hong and D.-W. Jee, "A 0.052 mm^2, <0.4% THD, sinusoidal current generator for bio-impedance measurement using a recursive digital oscillator and current-domain FIR filter," *IEEE Trans. Circuits Syst. II, Exp. Briefs*, vol. 66, no. 6, pp. 894–898, Jun. 2019.
[30] *Cree Screen Master 4-mm Oval LED C4SMM-RJY/GJY/BJY*. Accessed: Feb. 2020. [Online]. Available: https://cree-led.com/media/documents/C4SMM-1473.pdf
[31] R. R. Harrison, "The design of integrated circuits to observe brain activity," *Proc. IEEE*, vol. 96, no. 7, pp. 1203–1216, Jul. 2008.
[32] *Dissolved Oxygen: Hach LDO Probe, Model 2, Data Sheet LIT2455*. Accessed: Jan. 2014. [Online]. Available: https://www.hach.com/asset-get.download.jsa?id=7639981835

XUANKAI ZHI received the B.S. degree in microelectronics science and engineering from Nankai University, Tianjin, China, in 2018. He is currently pursuing the M.S. degree with the School of Information Science and Technology, Fudan University, Shanghai, China. His research interests include analog front-end circuit for sensor interfaces and power management IC design.

YATING ZOU received the B.S. degree in integrated circuit design and integration system from the University of Electronic Science and Technology of China (UESTC), Chengdu, China, in 2019. She is currently pursuing the M.S. degree with Fudan University, Shanghai, China. Her research interests include analog front-end circuit for sensor interfaces and data converters.

YIZHOU JIANG (Student Member, IEEE) received the B.Eng. degree in microelectronics from Fudan University, Shanghai, China, in 2018, where he is currently pursuing the Ph.D. degree with the School of Information Science and Technology. His research interests include smart sensing circuits and systems, wearable and implantable biomedical devices, hybrid integration of solid-state circuits with flexible electronics, and hardware implementation of AI algorithms.

YAJIE QIN (Member, IEEE) received the B.S. and M.S. degrees in microelectronics and the Ph.D. degree from Fudan University, Shanghai, China, in 2001 and 2005, respectively, and the Ph.D. degree from the KTH-Royal Institute of Technology, Stockholm, Sweden. He is currently an Associate Professor with the School of Information Science and Technology, Fudan University. His current research interests include analog and mixed-signal circuits, techniques to hybrid integrate IC with flexible electronics, mixed-mode VLSI systems for information processing, and wearable/ implantable systems for IoT-based healthcare. He served in the Organization Committee for the IEEE International Conference on ASIC, in 2011 and 2017.